Arrayed Waveguide Grating with Reusable Delay Lines (RDL-AWG) for High Resolving Power, Highly Compact, Photonic Spectrographs

YANG ZHANG,[1] PRADIP GATKINE,[2] JIAHAO ZHAN,[1] SYLVAIN VEILLEUX,[3] AND MARIO DAGENAIS[1,*]

[1] *Department of Electrical and Computer Engineering, University of Maryland, College Park, MD 20742, USA*
[2] *Department of Astronomy, California Institute of Technology, Pasadena, CA 91125, USA*
[3] *Department of Astronomy, University of Maryland, College Park, MD 20742, USA*
**dage@umd.edu*

Abstract: An innovative arrayed waveguide grating with reusable delay lines (RDL-AWG) was designed and experimentally demonstrated as a high resolving power integrated photonic spectrometer. An array of directional couplers is optimized to distribute the input signal from the delay lines into the free propagation region. This design is >100 times more compact than the traditional AWGs. By making the AWGs more compact, it significantly reduces the impact of fabrication imperfections and uniformity issues which prevent traditional AWGs from achieving ultra-high resolving powers. A resolving power of 95,000 was recently measured in an RDL-AWG with a footprint of 4.2 x 2.9 mm^2 and no phase compensation.

1. Introduction

Arrayed waveguide gratings have been extensively used in optical communication as wavelength routers, multiwavelength receivers, multiwavelength lasers, wavelength-selective switches and add-drop multiplexers [1]. They will also find applications in on-chip spectral-domain optical coherence tomography [2], optical sensors [3], neural networks [4], quantum information and astronomy. Astrophotonic spectrograph is an emerging field geared towards bringing the advantages of photonic integrated circuits (PICs) to astronomical spectroscopy [5,6]. These on-chip spectrographs can be made compatible with established CMOS processes and have demonstrated good performances in terms of throughput, spectral resolving power, polarization control, etc.

Among various implementations of photonic spectrographs, arrayed waveguide grating (AWG) is one of the most promising technologies, as it is relatively simpler in design and easier in fabrication [7–9]. The high efficiency of AWGs makes it more suitable for astrophotonic spectroscopy, and potentially as building blocks for cascaded structures. Multi-stage AWG and micro-ring resonator integrated AWG designs have also been studied for expanding the resolving power of a singular AWG [10–13].

However, as the resolving power ($R = \lambda / \Delta\lambda$, where $\Delta\lambda$ is 3-dB transmission bandwidth) increases, the footprint of the traditional AWG design increases monotonically, which incorporates two free propagation regions (FPRs) and an array of waveguides. The phase errors caused by fabrication variations are proportional to the device footprint, which leads to a degradation in device performance as the AWG resolving power increases [14,15]. Various approaches have been studied to reduce the impact of phase-error issues, including footprint reduction and active phase compensation [16,17]. When the number of arrayed waveguides increases to over 100, which is necessary for high resolving powers (R > 10,000), the active phase control requires complex digital circuits and high power consumption. The footprint reduction is typically achieved by overlapping the input and output FPRs or adding reflectors to the ends of the arrayed waveguides [18,19]. Either way could only reduce the footprint by a maximum factor of 2. Here, we introduce an innovative approach to design a much more compact AWG with reusable delay lines (RDL-AWG), which uses only one waveguide to bring accurate power and phase distributions into the output FPR.

The paper is organized as follows. In the following section, we will first briefly discuss the motivation for the RDL-AWG development and in Section 3, the theoretical design rules of RDL-AWGs will be provided. In Section 4, we will provide the details of the fabrication process of the device and the measurement set-up. The performance of fabricated devices will be analyzed in Section 5. Finally, the outlook towards future development and conclusions will be given in Section 6.

2. Motivation for RDL-AWG development

In a traditional AWG, the arrayed waveguides between two FPRs are constructed to introduce a constant path difference between adjacent waveguides. The longest waveguide is at least $\lambda \cdot R$, where λ is the operating wavelength and R is the resolving power [20]. This implies that to achieve a higher resolving power AWG spectrometer requires an increase in the optical path length of the arrayed waveguides. Not only does this result in an increase of the footprint of the device, but also, more importantly, it leads to optical phase errors that are generated by fabrication imperfections which can become a significant issue [14,15]. These phase errors degrade the performance of the device by deteriorating the shape of the peaks, and therefore, increase insertion loss and cross-talk, and limit the resolving power [21,22]. To alleviate this issue, active corrections of waveguide phase errors based on integrating electro-optic or thermo-optic phase shifters in high-R AWGs are typically used [17,23]. However, incorporating a phase shifter into every waveguide of the device would significantly increase the size, weight, power consumption, and cost (Swap-C) of the device. It also brings complexity to the chip fabrication and the testing of the AWG.

To break the ultimate limitation in achieving high-R, we present an AWG with reusable delay lines, see Fig. 1. Unlike the traditional AWGs, where the phase distribution is introduced by an array of waveguides with different lengths between two FPRs, one single waveguide is used to provide both the power and phase distribution by an array of embedded directional couplers (DCs). The transmitted power and phase of each DC in the array is controlled by both the gap width and the coupling length. With the capability to fabricate sub-10 nm feature size by electron-beam (E-beam) lithography, the arrayed DCs can generate arbitrary power and phase distribution required to illuminate the output FPR. In this paper, to prove the concept, a power and phase distribution that are the same as the traditional AWG are generated by the arrayed DCs. The footprint of the spectrometer is reduced by a factor of more than 100. It eliminates the need for making large AWGs and the associated step of actively compensating the phase error.

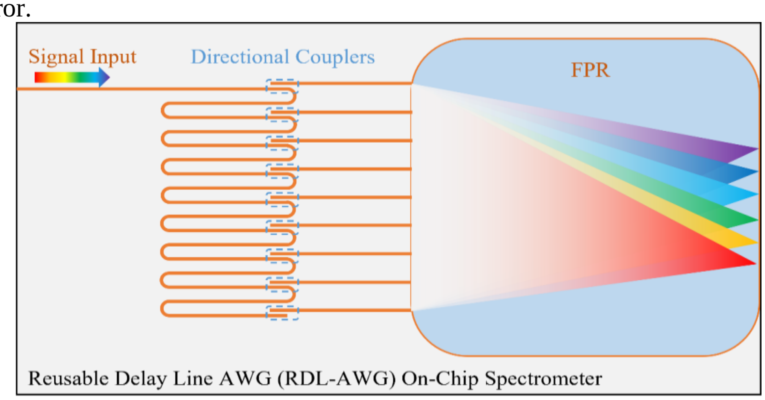

Fig. 1 A schematic of the arrayed waveguide grating with reusable delay lines (RDL-AWG).

3. Theoretical design of RDL-AWG

The design flow of the embedded array of DCs is shown in Fig. 2 (a). The purpose of the arrayed DCs is to generate the power and phase distribution that feed into the FPR shown in Fig. 1. Both the required power and phase distribution presented in this work are the same as those of the output FPR in the traditional AWG. A traditional AWG is simulated by Rsoft to get the proper phase distribution. The power distribution is simply a Gaussian distribution, while the phase distribution can be treated as an array of 0's at the central wavelength λ_0. For the other wavelengths, the phase is a linear distribution depending on the grating orders. The power and phase look-up table of the DCs is simulated by the Beam Propagation Method in Rsoft, and further modified by experimental data. It contains the values of β, θ_1, θ_2 for different coupling lengths L, as shown in Fig. 2 (b), where β is the remaining power coefficient, θ_1 is the extra phase introduced in the bus of the DC, θ_2 is the extra phase introduced in the coupler of the DC. In this work, the gap width of the DC is 0.6 um. Then, the two databases are used to calculate the lists of coupler length L and extra path P, shown in Fig. 2 (a), where the extra path P is used to correct the phase distribution caused by θ_1 and θ_2. To demonstrate how we use the lists of L and P to construct the new AWG structure, two examples of the implementations are shown.

The optical path difference ΔL is set by the grating order m ($\Delta L = m \times \lambda_0$), which is directly related to the resolving power (R) by $R \approx m \times N$, where N is the number of waveguides in the array. After the calculation of the L and P lists, to change the R value, the only parameter that needs to be changed is ΔL. This makes the design process simple and fast. We note that by adjusting both the phase and the power distribution of the light in the waveguides, we can generate different input profiles. For example, a flat-top transmission profile for each of the output channels can be achieved by altering the power distribution [20,24].

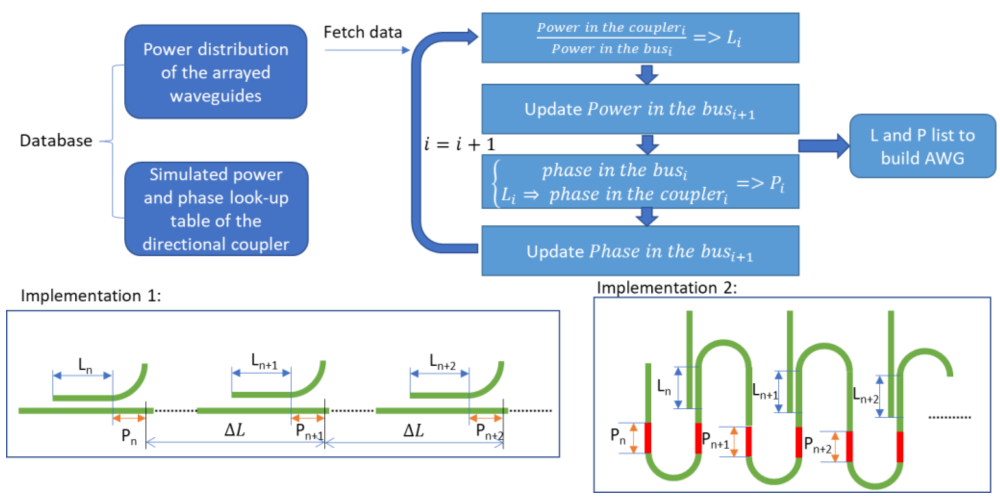

(a)

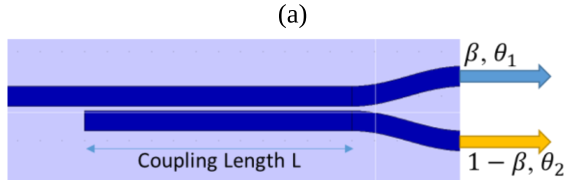

(b)

Fig. 2 (a) Flowchart to calculate the directional coupler array position P and length L. (b) Power and phase simulated in a directional coupler.

A model is established to accurately measure the parameters β, θ_1, θ_2, which is based on the Mach–Zehnder interferometer (MZI), as shown in Fig. 3 (a). A MZI constructed with two identical 2×2 multi-mode interferometers (MMIs) is designed as the baseline structure to extract the α that is the property of the MMIs. It also works as a reference to eliminate any extra losses, like propagation loss, fiber-waveguide coupling loss, etc. In Fig. 3 (b), one directional coupler with coupling length L is added to the upper arm of the MZI. The rest of the test structure is the same as the baseline structure. This ensures that there is no extra phase or power disturbance in the MZI. By measuring the output power P_{DC}, we can extract the value of β, based on the equation,

$$P_{DC} = P_{in} \cdot \alpha_1 \cdot (1-\beta) \tag{1}$$

Fig. 3 (c) shows the extracted $1-\beta$ as a function of coupler length L. Then, θ_1 can be evaluated for a measured P_{MZI}, based on the equation,

$$P_{MZI} = P_{in} \cdot \alpha_1 \cdot \alpha_2 \cdot \left|(\sqrt{\beta} \cdot e^{j(\theta_1+\phi)} + e^{j\phi})\right|^2 \tag{2}$$

Fig. 3 (d) shows the extracted θ_1 as a function of coupler length L. Finally, θ_2 can be extracted by fitting θ_1 as a function of coupling length L in the theory.

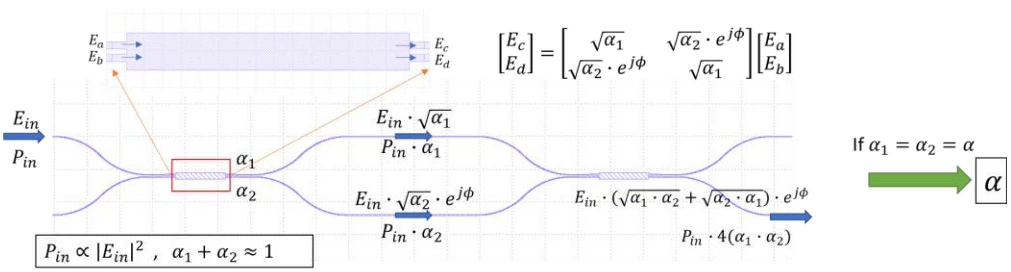

(a)

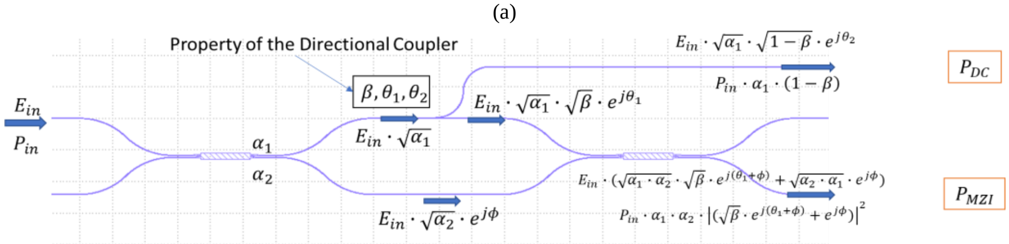

(b)

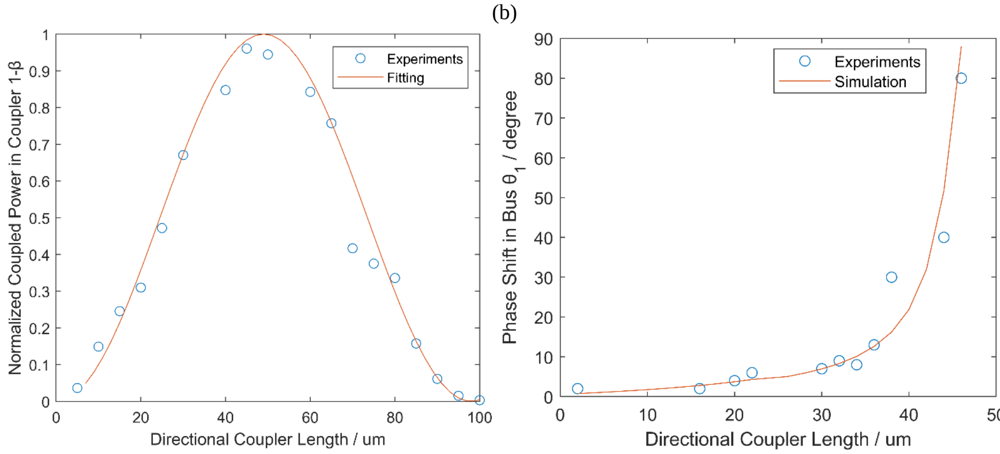

(c) (d)

Fig. 3 (a) Baseline structure to extract α. (b) Test structure to extract β, θ_1. (c) (1- β) as a function of coupler length L. (d) Phase shift in bus θ_1 as a function of coupler length L.

Table. 1 Summary of the design specs of the two RDL-AWGs

	RDL-AWG #1	RDL-AWG #2
Waveguide cross-section	1.0 µm × 0.3 µm	1.0 µm × 0.3 µm
Number of waveguides	20	20
Grating order	1600	8000
FSR @1550 nm	0.91 nm	0.182 nm
ΔL	1637.372 µm	8186.860 µm
Number of outputs	8	8
Targeted resolving power	30,000	120,000
Minimum radius of curvature	60 µm	60 µm
Footprint	0.9 × 2.9 mm^2	4.2 × 2.9 mm^2

In this paper, two RDL-AWG designs based on the above calculations are generated, as shown in Fig. 4 (a), with targeted resolving power of 30,000 and 120,000, respectively. We will refer to the two designs as RDL-AWG #1 and RDL-AWG #2 in the following content. The design specs are summarized in Table. 1. As proof-of-concept RDL-AWGs, the number of arrayed waveguides is 20 for both designs, and the number of the output channels is chosen to be 8. While the current proof-of-concept design has a limited free spectral range (FSR), the design easily allows more arrayed waveguides and output channels to be added to increase the FSR. The footprints of the devices are 0.9 × 2.9 mm^2 and 4.2 × 2.9 mm^2, respectively. The footprints of the devices are reduced by more than 100 times compared to the traditional AWGs, as shown in Fig. 4 (b). It is worth mentioning that we are comparing the footprint of RDL-AWGs and traditional AWGs with the same number of arrayed waveguides and grating orders, with the same thickness of Si_3N_4.

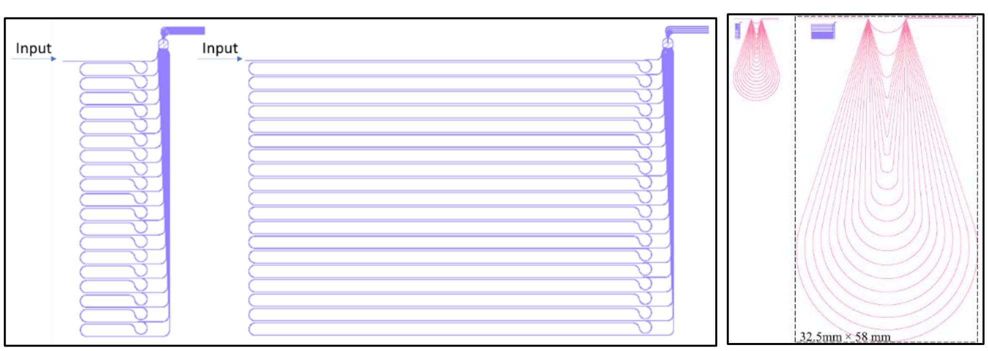

(a) (b)

Fig. 4 (a) Two RDL-AWG designs with targeted resolving power of 30,000 and 120,000, respectively. (b) The comparison between the RDL-AWGs and traditional AWGs. The purple ones are the RDL-AWGs. The red ones are the traditional AWGs.

4. Fabrication and measurement

The PIC was fabricated on a Si_3N_4/SiO_2 on silicon platform, which provides benefits such as low optical losses, transparency over a wide wavelength range (400-2350 nm), compatibility with CMOS, and wafer-scale foundry processes. The structure used in this paper has layers of 10-um thermal SiO_2 as the bottom cladding, 300-nm Si_3N_4 deposited by low pressure chemical vapor deposition (LPCVD) as the core layer, and 3-um SiO_2 deposited by plasma enhanced chemical vapor deposition (PECVD) as the top cladding. Compared to thinner Si_3N_4 films, this geometry has lower bending losses in waveguides with small radii of curvature (for a 60-um-radius bend, the bending loss is 0.37 dB/m), which allows us to design ultra-compact RDL-AWGs. The RDL-AWG design was patterned by a 100 keV Elionix ELS-G100 e-beam system. A 10-nm Cr film was deposited as the mask to etch the 300-nm Si_3N_4 layer. Compared to the traditional AWGs, the process of etching is more critical in RDL-AWGs, as the transmitted power and phase of the directional couplers are sensitive to the etching depth and quality (sidewall roughness). To achieve the expected power and phase distribution to the output FPR, the etching rate needs to be carefully calibrated.

The setup to characterize the transmission response of the RDL-AWGs is shown in Fig. 5. A polarization maintaining tunable laser source (Keysight, 81607A) operating over a wavelength range of 1450 nm − 1640 nm was used, which has a narrow linewidth (0.1 pm) and a high signal to total source spontaneous emission ratio (>70 dB). A polarization maintaining single mode fiber (PM1550) with a typical mode-field diameter of 10.1 µm and a numerical aperture of 0.125 was used to carry the signal from the tunable laser source to the RDL-AWG and out to the power meter. The polarization of the signal entering the RDL-AWG was controlled by a high precision fiber rotator (Thorlabs, HFR007). The fibers were butt-coupled to the PIC using the precision 3-axis stages (< 100 nm alignment tolerance). A power meter (Keysight, N7744A) with a dynamic range of 65 dB was used to analyze the transmitted signal.

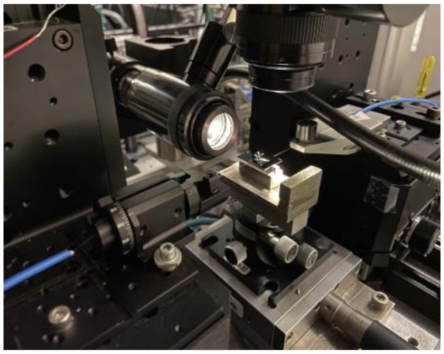

Fig. 5 Setup used to measure the transmission spectrum.

5. Device Characterization

The transmission response of each output channel of the RDL-AWGs was measured using the measurement setup described in Section 4 and shown in Fig. 5. The overall throughput of the two RDL-AWGs is plotted as a function of wavelength in Fig. 6.

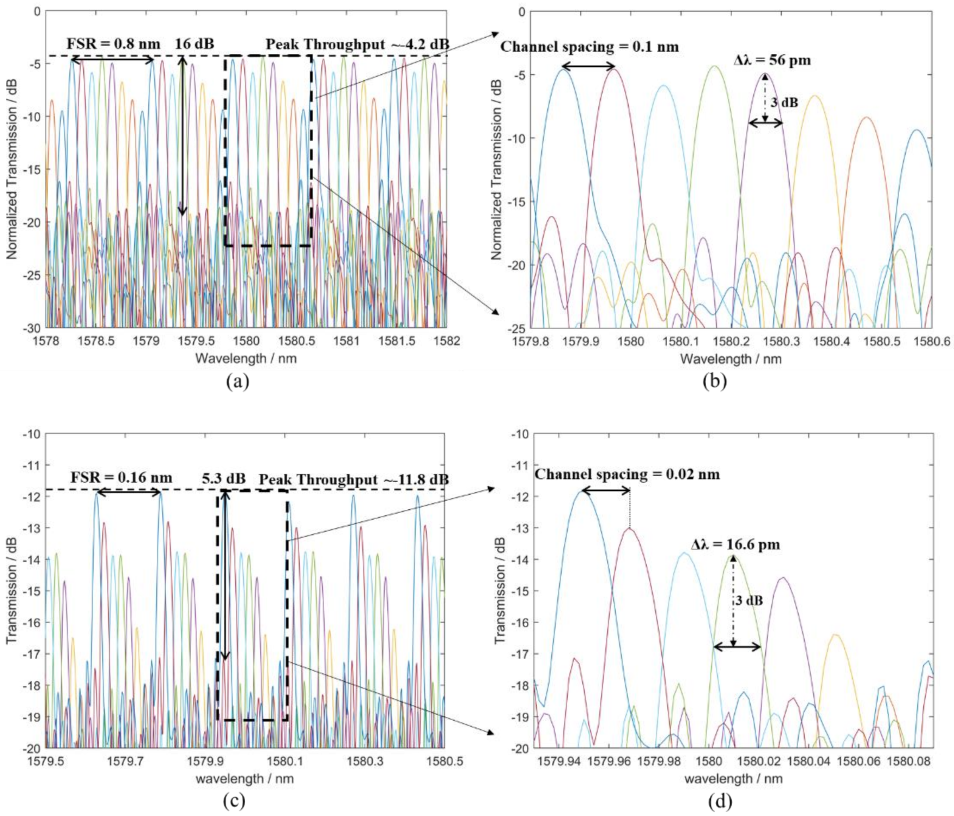

Fig. 6 Transmission spectra of RDL-AWGs. (a), (b): RDL-AWG #1 with a targeted R of 30,000. (c), (d): RDL-AWG #2 with a targeted R of 120,000.

For the RDL-AWG #1 with a targeted R of 30,000, shown at Fig. 6 (a) and (b), the throughput is measured to be -4.2 dB in the wavelength bandwidth of 1575 – 1580 nm. We measure a FSR of 0.8 nm and a crosstalk of ~16 dB. The channel spacing between output channels is measured to be 0.1 nm, and the 3-dB transmission bandwidth is 56 pm, corresponding to a resolving power of 28,000 at 1580 nm. With the capability to fabricate the device in a compact area (0.9×2.9 mm^2) and with ultra-low-loss waveguide (<0.02 dB/cm) [25,26], we therefore achieve a resolving power that is in good agreement with the theoretical value. Note that the throughput can even be increased by using high coupling efficiency fiber-to-waveguide couplers [27] with mode-matching ultra-high numerical aperture (UHNA) fibers or lensed fibers.

Figs. 6 (c) and (d) show the transmission response for the RDL-AWG #2 with a targeted R of 120,000. The throughput is measured to be -11.8 dB, which is 7.6 dB lower than that of RDL-AWG #1. We also see that the crosstalk is ~5.3 dB, which is also poorer than that of RDL-AWG #1. The degradation of both throughput and crosstalk are mostly due to the phase errors introduced by the fabrication process in a larger area (4.2×2.9 mm^2), which depends on the stability of the fabrication process across the dispersive area of the device. The small footprint RDL-AWG device helps to minimize phase errors. In the future, better process control can alleviate this issue further. As a result, the measured resolving power of RDL-AWG #2 is 95,000, in contrast to the targeted value of 120,000.

6. Discussion and Conclusion

The innovative RDL-AWG design presented in this work has unique advantages over traditional AWGs for achieving a high resolving power. An array of directional couplers is calculated and optimized to distribute the input signal from the delay line into the free propagation region. By making the AWGs more compact, it significantly reduces the impact of fabrication imperfections and uniformity issues, which limit the traditional AWGs from achieving ultra-high resolving powers. The design theory is discussed in detail. We also experimentally demonstrate devices with resolving powers of 28,000 and 95,000. These devices are more than 100 times more compact compared to the traditional AWGs.

The presented preliminary RDL-AWGs have only 20 arrayed waveguides and 8 output channels. The experimental results show that the concept to reuse the delay line to reduce the footprint works well. The next step is to build an RDL-AWG with a larger number of arrayed waveguides and output channels, which means a higher FSR. A challenge to note is the loss due to the DCs. As the number of arrayed waveguides in the RDL-AWG increases, the number of arrayed DCs also increases accordingly. For example, if the loss of a single DC is estimated to be 0.01 dB, for a 20-waveguide RDL-AWG, the estimated loss due to arrayed DCs will be 0.095 dB. For a 100-waveguide RDL-AWG, the loss will be 0.489 dB. This is an extra source of loss which does not exist in traditional AWGs. Careful engineering and optimization of the DCs are required in future developments.

In this paper, we demonstrated the RDL-AWGs on a 300-nm thick Si_3N_4 core layer. It provides a lower bending loss compared to other waveguide geometries that have relatively lower confinement factors. This in turn makes it possible to design RDL-AWGs with smaller footprints, which are less susceptible to fabrication variations. To further reduce the minimum bending radii, a thicker Si_3N_4 core layer can be used [21], which makes the RDL-AWG a more compelling approach for compact higher-resolution spectrometers.

The power and phase distribution can be arbitrarily generated by the arrayed DCs. This means that the output spectrum can be altered to achieve various peak profiles. Besides the traditional Gaussian, a flat-top shape is one of the preferred options [24].

As discussed in Section 5, by comparing the performance of the two RDL-AWG designs presented in this paper, the design with higher R starts to be affected by phase errors due to a larger footprint. This phenomenon is similar to the performance degradation of traditional AWGs fabricated on the 300-nm Si_3N_4/SiO_2 platform, when the resolving power is larger than 10,000. For the higher-R designs, a delay line that fits in a more compact area is required. We are currently working on a new structure that utilizes an array of spiral delay lines. It has the potential to further reduce the size of the RDL-AWG with R>100,000 by a factor of 5.

Funding. National Science Foundation under grant 1711377, the National Aeronautics and Space Administration (NASA) under grant 16-APRA 16-0064, and a NASA Hubble Fellowship HST-HF2-51478.001-A.

Acknowledgments. We acknowledge the support of the Maryland NanoCenter and its FabLab. Support for P. Gatkine was provided by NASA through the NASA Hubble Fellowship grant HST-HF2-51478.001-A awarded by the Space Telescope Science Institute, which is operated by the Association of Universities for Research in Astronomy, Incorporated, under NASA contract NAS5-26555.

Disclosures. The authors declare no conflicts of interest.

Data availability. Data underlying the results presented in this paper are not publicly available at this time but may be obtained from the authors upon reasonable request.

References

1. M. K. Smit and C. Van Dam, "PHASAR-based WDM-devices: Principles, design and applications," IEEE Journal of Selected Topics in Quantum Electronics **2**, 236–250 (1996).
2. Z. Zhang, Y. Wang, and H. K. Tsang, "Ultracompact 40-Channel Arrayed Waveguide Grating on Silicon Nitride Platform at 860 nm," IEEE Journal of Quantum Electronics **56**, 1–8 (2020).

3. A. Z. Subramanian, E. Ryckeboer, A. Dhakal, F. Peyskens, A. Malik, B. Kuyken, H. Zhao, S. Pathak, A. Ruocco, A. De Groote, P. Wuytens, D. Martens, F. Leo, W. Xie, U. D. Dave, M. Muneeb, P. Van Dorpe, J. Van Campenhout, W. Bogaerts, P. Bienstman, N. Le Thomas, D. Van Thourhout, Z. Hens, G. Roelkens, and R. Baets, "Silicon and silicon nitride photonic circuits for spectroscopic sensing on-a-chip [Invited]," Photon. Res. **3**, B47 (2015).
4. S. Chen, S. Chen, F. Yao, F. Yao, S. Ren, S. Ren, G. Wang, G. Wang, G. Wang, M. Huang, M. Huang, and M. Huang, "Cost-effective improvement of the performance of AWG-based FBG wavelength interrogation via a cascaded neural network," Opt. Express, OE **30**, 7647–7663 (2022).
5. J. Bland-Hawthorn and P. Kern, "Astrophotonics: a new era for astronomical instruments," Opt. Express, OE **17**, 1880–1884 (2009).
6. P. Gatkine, S. Veilleux, and M. Dagenais, "Astrophotonic Spectrographs," Applied Sciences **9**, 290 (2019).
7. N. Cvetojevic, N. Jovanovic, J. Lawrence, M. Withford, and J. Bland-Hawthorn, "Developing arrayed waveguide grating spectrographs for multi-object astronomical spectroscopy," Opt. Express **20**, 2062 (2012).
8. P. Gatkine, S. Veilleux, Y. Hu, T. Zhu, Y. Meng, J. Bland-Hawthorn, and M. Dagenais, "Development of high resolution arrayed waveguide grating spectrometers for astronomical applications: first results," arXiv:1606.02730 [astro-ph, physics:physics] 991271 (2016).
9. P. Gatkine, S. Veilleux, Y. Hu, J. Bland-Hawthorn, and M. Dagenais, "Arrayed Waveguide Grating Spectrometers for Astronomical Applications: New Results," Opt. Express **25**, 17918 (2017).
10. A. van Wijk, C. R. Doerr, Z. Ali, M. Karabiyik, and B. I. Akca, "Compact ultrabroad-bandwidth cascaded arrayed waveguide gratings," Opt. Express, OE **28**, 14618–14626 (2020).
11. K. Takada, M. Abe, T. Shibata, and K. Okamoto, "A.2.5 GHz-spaced 1080-channel tandem multi/demultiplexer covering the. S-, C-, and L-bands using an arrayed-waveguide grating with Gaussian passbands as a primary filter," IEEE Photonics Technology Letters **14**, 648–650 (2002).
12. Z. Zhang, Y. Wang, and H. K. Tsang, "Tandem Configuration of Microrings and Arrayed Waveguide Gratings for a High-Resolution and Broadband Stationary Optical Spectrometer at 860 nm," ACS Photonics **8**, 1251–1257 (2021).
13. S. Zheng, H. Cai, J. Song, J. Zou, P. Y. Liu, Z. Lin, D.-L. Kwong, and A.-Q. Liu, "A Single-Chip Integrated Spectrometer via Tunable Microring Resonator Array," IEEE Photonics Journal **11**, 1–9 (2019).
14. T. Goh, S. Suzuki, and A. Sugita, "Estimation of waveguide phase error in silica-based waveguides," Journal of Lightwave Technology **15**, 2107–2113 (1997).
15. T. Kamalakis, T. Sphicopoulos, and D. Syvridis, "An estimation of performance degradation due to fabrication errors in AWGs," Journal of Lightwave Technology **20**, 1779–1787 (2002).
16. H. Yamada, "Crosstalk Reduction in a 10-GHz Spacing Arrayed-Waveguide Grating by Phase-Error Compensation," J. Lightwave Technol., JLT **16**, 364 (1998).
17. M. Gehl, D. Trotter, A. Starbuck, A. Pomerene, A. L. Lentine, and C. DeRose, "Active phase correction of high resolution silicon photonic arrayed waveguide gratings," Opt. Express, OE **25**, 6320–6334 (2017).
18. K. Okamoto and K. Ishida, "Fabrication of silicon reflection-type arrayed-waveguide gratings with distributed Bragg reflectors," Opt. Lett., OL **38**, 3530–3533 (2013).
19. H. Hu, Q. Fang, S. Wang, X. Zhang, X. Ma, M. Gu, L. Jia, and H. Chen, "Folded 15-channel arrayed waveguide gratings on silicon nitride platform with loop reflector," Optics Communications **500**, 127321 (2021).
20. K. Okamoto, *Fundamentals of Optical Waveguides*, Third (2022).
21. P. Gatkine, N. Jovanovic, C. Hopgood, S. Ellis, R. Broeke, K. Ławniczuk, J. Jewell, J. K. Wallace, and D. Mawet, "Potential of commercial SiN MPW platforms for developing mid/high-resolution integrated photonic spectrographs for astronomy," Appl. Opt. **60**, D15 (2021).
22. A. Stoll, K. Madhav, and M. Roth, "Performance limits of astronomical arrayed waveguide gratings on a silica platform," Opt. Express, OE **28**, 39354–39367 (2020).
23. W. Jiang, N. K. Fontaine, F. Soares, J. H. Baek, K. Okamoto, S. Yoo, F. Olsson, and S. Lourdudoss, *Dynamic Phase-Error Compensation for High-Resolution InP Arrayed-Waveguide Grating Using Electro-Optic Effect* (2008), p. 54.
24. K. Okamoto and H. Yamada, "Arrayed-waveguide grating multiplexer with flat spectral response," Opt. Lett., OL **20**, 43–45 (1995).
25. Y. Zhang, J. Zhan, S. Veilleux, and M. Dagenais, "Silicon Nitride Fabry-Perot Bragg Grating Nanoresonator with Ultrahigh Intrinsic Q," in *2022 Conference on Lasers and Electro-Optics (CLEO)* (2022), pp. 1–2.
26. Y.-W. Hu, Y. Zhang, P. Gatkine, J. Bland-Hawthorn, S. Veilleux, and M. Dagenais, "Characterization of Low Loss Waveguides Using Bragg Gratings," IEEE Journal of Selected Topics in Quantum Electronics **24**, 1–8 (2018).
27. T. Zhu, Y. Hu, P. Gatkine, S. Veilleux, J. Bland-Hawthorn, and M. Dagenais, "Ultrabroadband High Coupling Efficiency Fiber-to-Waveguide Coupler Using Si_3N_4/SiO_2Waveguides on Silicon," IEEE Photonics Journal **8**, 1–12 (2016).